

SPECTROSCOPIC STUDY OF BLUE STRAGGLER STARS IN THE GLOBULAR CLUSTER NGC 3201

Gourav Kumawat^{1,2}, Arvind K. Dattatreya³, R.K.S. Yadav³

Draft version: May 22, 2025

RESUMEN

Favor de proporcionar un resumen en español. If you are unable to translate your abstract into Spanish, the editors will do it for you.

ABSTRACT

We conducted a spectroscopic study of 39 blue straggler stars in the globular cluster NGC 3201. The spectra of these stars were collected from the literature. We determined the radial velocity, atmospheric parameters (T_{eff} , $\log g$), and the abundance of Mg, as well as the metallicity ([Fe/H]) of the blue straggler population. The mean radial velocity and [Fe/H] are determined to be 498.0 ± 5.3 km/s and -1.42 ± 0.27 , respectively, for the blue straggler stars. The derived [Fe/H] is consistent, within uncertainties, with the cluster's [Fe/H] of -1.59 dex. The mean [Mg/Fe] for the blue straggler stars is estimated to be 0.36 ± 0.73 . Importantly, this study first estimates [Mg/Fe] for the blue straggler stars in the cluster NGC 3201.

Key Words: Blue Straggler Stars — Globular star clusters: NGC 3201 — Spectroscopy

1. INTRODUCTION

Globular clusters (GCs) are among the oldest stellar systems, consisting of thousands of stars located at the same distance from us and moving together in space. Due to their high stellar densities, frequent gravitational interactions occur within them, leading to several dynamical processes that give rise to exotic stellar populations. One such population is that of Blue Straggler stars (BSSs).

BSSs are identified as stars positioned to the left and above the main-sequence turnoff (MSTO) in the optical color-magnitude diagram (CMD). They were first discovered by Sandage (1953) in the GC M3. The position of BSSs in the CMD suggests that they are more massive than the current cluster members. This is further supported by previous mass measurements (Shara et al. 1997; Gilliland et al. 1998; Fiorentino et al. 2014). However, GCs are completely devoid of gas, making any recent star formation practically implausible. As a result, the origin of BSSs is associated with a mechanism that increases the initial stellar mass through a rejuvenation process. The two primary formation mechanisms of BSSs are mass transfer (MT) from an evolved donor to a lower-mass binary companion (McCrea 1964) and stellar collisions leading to mergers in high-density environments (Hills & Day 1976; Leonard 1989). The absence of a single formation scenario that explains all

¹Indian Institute of Science Education and Research, Bhopal, MP, INDIA.

²University of Alberta, Edmonton, AB, CANADA

³Aryabhatta Research Institute of Observational Sciences, Nainital, UK, INDIA

TABLE 1

IDs, RA, DEC, VISUAL MAGNITUDE, AND MEMBERSHIP PROBABILITY OF THE 39 BSSs USED IN THIS STUDY (REFER TO TEXT FOR DETAILS)

BSS ID	Cosmic-Lab ID	RA (degrees)	DEC (degrees)	m_V	PROB (%)
B1	1023539	154.3993515	-46.4078560	17.54	97
B2	1013700	154.3962520	-46.4182565	17.27	96.9
B3	1025211	154.3849299	-46.4076830	17.58	97.3
B4	1021152	154.4195717	-46.4093147	17.17	97.3
B5	1025619	154.3816172	-46.4041477	16.86	99.9
B6	1031149	154.4004033	-46.3970078	16.69	97.7
B7	1010831	154.4189046	-46.4216023	16.34	97.3
B8	1021331	154.4184729	-46.4027317	17.39	97.7
B9	1009786	154.4276377	-46.4137044	16.95	97.7
B10	1020369	154.4272846	-46.4087656	17.20	97.1
B11	1031222	154.3994121	-46.3927124	17.58	97.7
B12	1026151	154.3766105	-46.4000632	17.77	97.2
B13	1016643	154.3700469	-46.4114471	17.22	97.1
B14	1006762	154.3834415	-46.4321004	16.60	97.3
B15	1009269	154.4330228	-46.4137157	16.64	97.5
B16	1016923	154.3668729	-46.4150062	17.82	97.4
B17	1002749	154.4246075	-46.4282995	17.60	97.3
B18	1008650	154.4390510	-46.4182480	17.45	95.3
B19	1030901	154.4032020	-46.3843063	17.47	100
B20	2716018	154.3760880	-46.4361699	17.19	100
B21	2711709	154.4041397	-46.4461522	17.74	0.06
B22	1035238	154.3842813	-46.3772396	17.38	100
B23	2714632	154.3860264	-46.4501061	16.43	100
B24	2705506	154.4472108	-46.3887971	17.54	99.9
B25	2714006	154.3898416	-46.3689811	17.51	100
B26	2709841	154.4152943	-46.3652141	17.59	99.9
B27	2720497	154.3341108	-46.4439012	16.49	100
B28	2710692	154.4103191	-46.4691207	17.36	100
B29	2711836	154.4034550	-46.4747336	17.25	99.9
B30	2600533	154.3140993	-46.3867423	17.19	100
B31	2702518	154.4824695	-46.3775296	16.63	100
B32	2707141	154.4338850	-46.3495438	17.25	96.5
B33	2717272	154.3667567	-46.4837663	17.85	99.9
B34	2601851	154.2893054	-46.4032201	17.46	100
B35	2708408	154.4249930	-46.3192117	17.42	100
B36	2603838	154.2324762	-46.3496011	17.36	100
B37	2714749	154.3855481	-46.5545236	17.20	100
B38	2301092	154.2432987	-46.2935999	16.85	0
B39	2801544	154.6364229	-46.4157168	17.64	100

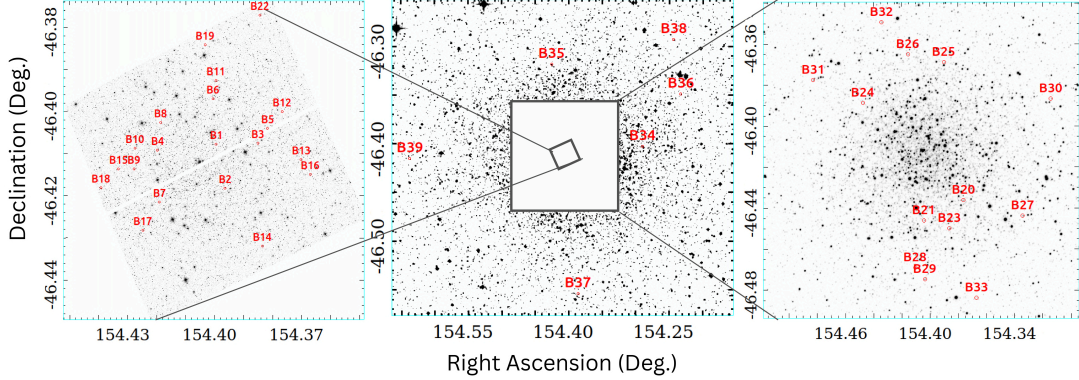


Fig. 1. Spatial locations of the BSSs in different regions of NGC 3201. The BSSs are marked with red circles and labelled with their IDs in all the images. **Left:** HST F606W image of the core of NGC 3201 taken by the HST ACS Wide Field Camera on March 14, 2006, with a total exposure time of 5 seconds (Nardiello et al. 2018). **Middle:** UK Schmidt telescope image of NGC 3201 taken on March 4, 1978, with a total exposure of 4200 seconds sourced from the DSS survey produced at the Space Telescope Science Institute (STScI). **Right:** ESO/MPG 2.2m telescope image of NGC 3201 in the V/89 filter taken by wide-field imager (WFI) with a total exposure of 480 seconds (credits: ESO Imaging Survey).

observed BSSs across different clusters necessitates identifying distinguishing characteristics for each formation scenario.

Chemical abundance is one such indicator that distinguishes the BSS formation scenario. Smooth particle hydrodynamics calculations reveal that stellar collisions produce merged objects with surface abundances matching the envelope of the most massive star (Lombardi Jr. et al. 1995). In contrast, binary mass transfer exposes and accretes the donor star's deeper layers, resulting in surface abundances indicative of partial hydrogen burning. For instance, in 47 Tuc, Ferraro et al. (2006) found many BSSs depleted in carbon (C) and oxygen (O), suggesting they accreted CNO-processed material from binary companions. Such chemical anomalies may indicate mass-transfer mechanisms. Notably, 47 Tuc shows a high prevalence of depleted BSSs, unlike clusters like M4, M30, and ω Centauri, where only a few stars show a C-O signature (Lovisi et al. 2010, 2013; Mucciarelli et al. 2014). Small numbers of CO-depleted BSSs suggest that mass transfer is either inefficient in GCs or C and O depletion is transient (Ferraro et al. 2006).

Billi et al. (2023) employed high-resolution spectra of BSSs in NGC 3201 obtained with the Magellan Telescope to determine their rotational velocities. They determined the effective temperature and surface gravity using isochrone fitting on the CMD locations of the BSSs. In this work, we aim to determine the radial velocity, atmospheric parameters and chemical abundances of the BSSs using the synthetic spectral fitting method.

NGC 3201 is a low galactic latitude halo GC in the southern constellation of Vela. The right ascension (RA) and declination (DEC) of the cluster center are $10^h 17^m 36.82^s$ and $-46^\circ 24' 44.9''$, respectively. The cluster has an age $\approx 12.2 \pm 0.5$ Gyr (Monty et al. 2018), a distance ≈ 4.9 kpc, metallicity $[\text{Fe}/\text{H}] \approx -1.59$ dex, and reddening ≈ 0.24 mag (Harris 1996).

The article is structured as follows: § 2 describes the data sets used in this study. The methodology is presented in § 3. The results of this study are described in § 4, while § 5 presents the conclusions.

2. DATA

In this work, we have used BSS spectra, along with their corresponding RA & DEC and $v \sin(i)$ values, which are openly available at Cosmic-lab⁴. The spectra were acquired from the multi-object fiber system Michigan/Magellan Fiber System (M2FS), which feeds the double spectrograph MSPec mounted on the Magellan Clay Telescope at the Las Campanas Observatory in Chile. The spectra were acquired as part of the proposal CN2019A-15 with Principal Investigator Lorenzo Monaco. The M2FS instrument enables the simultaneous observation of up to 128 objects per spectrograph over a FOV of about 30' in diameter. The data were collected in February-March 2019 through 16 repeated exposures in the spectral region 5127–5184 Å, with a spectral resolution of 18000. This resolution allowed us to adequately sample the first two lines of the Mg triplet at 5167.3 Å and 5172.6 Å. Two distinct fiber configurations were utilized to obtain spectra for roughly 200 targets in the direction of the cluster. Our analysis targeted objects with spectra that reached an optimal Signal-to-Noise ratio (S/N) of ~ 40 –50. A total of six exposures, each lasting 30 minutes, were acquired on the first night, while 10 exposures, each lasting 20 minutes, were obtained on the second night (Billi et al. 2023). Billi et al. (2023) provides a detailed description of the data reduction process and their methodology for determining radial velocity, cluster membership, atmospheric parameters, and $v \sin(i)$ values for the BSSs.

Out of the 67 BSSs analyzed by Billi et al. (2023), we used 39 BSSs for which we were able to sample the Mg and Fe lines (see Table 2) for proper atmospheric parameters and chemical abundance estimation. The ID, RA, DEC, visual magnitude, and cluster membership probability for these 39 BSSs can be found in Table 1. The BSS IDs are named such that smaller numbers correspond to BSSs closer to the cluster's core. The Cosmic-Lab ID, RA and DEC are directly taken from the Cosmic-Lab website. The apparent visual magnitude (m_V) is obtained by crossmatching the BSSs positions with the photometric catalogue of the Stetson database (Stetson et al. 2019). The cluster membership probabilities (PROB) are obtained from Nardiello et al. (2018) and Vasiliev & Baumgardt (2021).

The spatial locations of these BSSs in different cluster regions can be seen in Figure 1. Out of the total 39 BSSs used in this study, 13 are within the core radius ($R_c = 1.3'$), 13 lie between the core and half-light radii, and 13 are beyond the half-light radius ($R_h = 3.1'$) of NGC 3201 (Harris 1996). The continuum-normalized and radial velocity-corrected spectra of the BSSs are given in Figure 2.

3. METHODOLOGY

We utilized **iSpec** (Blanco-Cuaresma et al. 2014; Blanco-Cuaresma 2019) for spectral analysis in our work. **iSpec** is an integrated spectroscopic software framework⁵ designed for determining

⁴http://www.cosmic-lab.eu/Cosmic-Lab/BSS_rotation.html

⁵<https://www.blancocuaresma.com/s/iSpec>

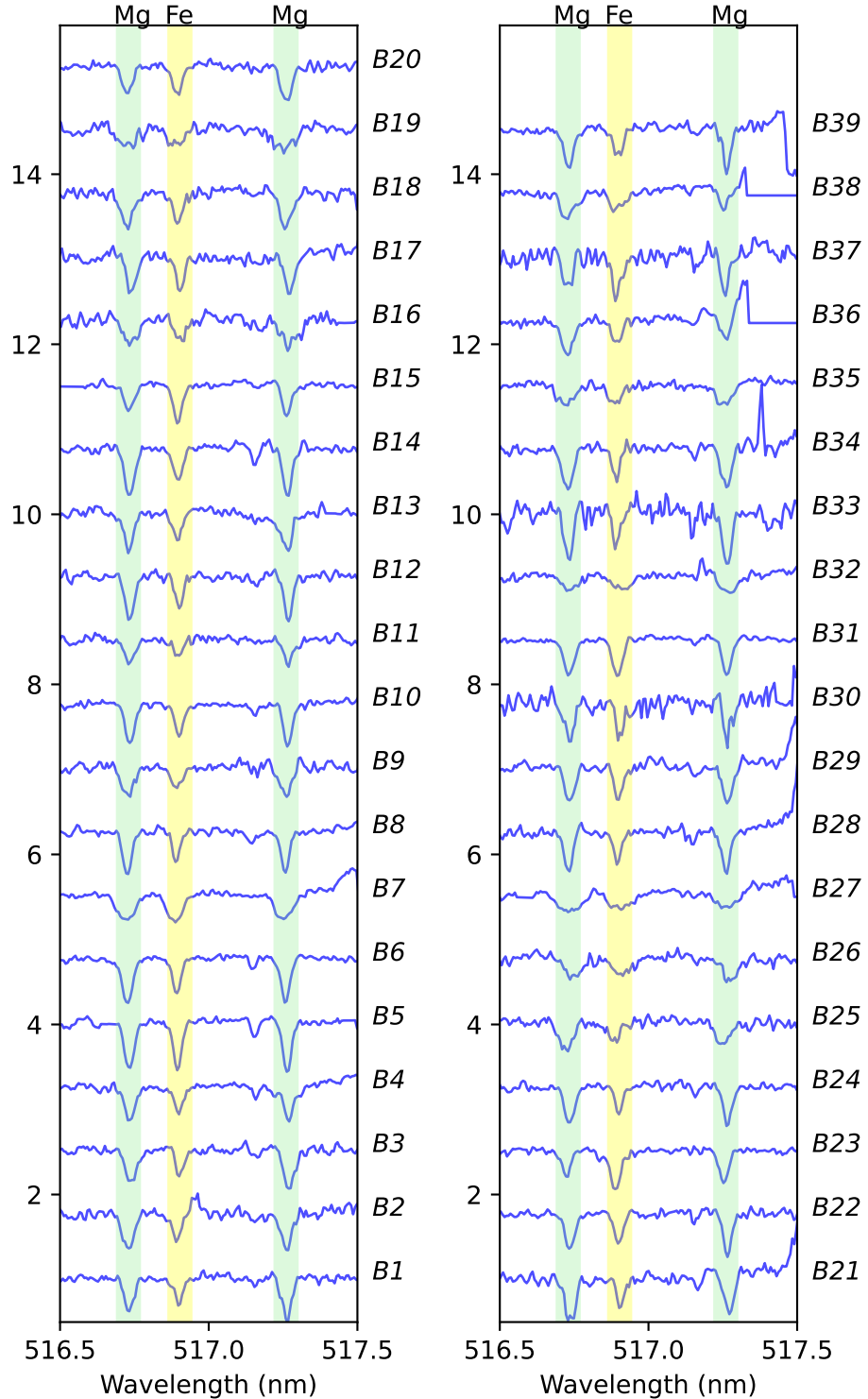


Fig. 2. The normalized and radial velocity-corrected spectra of 39 BSSs (B1-B39) of the cluster NGC 3201. The Mg and Fe lines are shown with vertical bands.

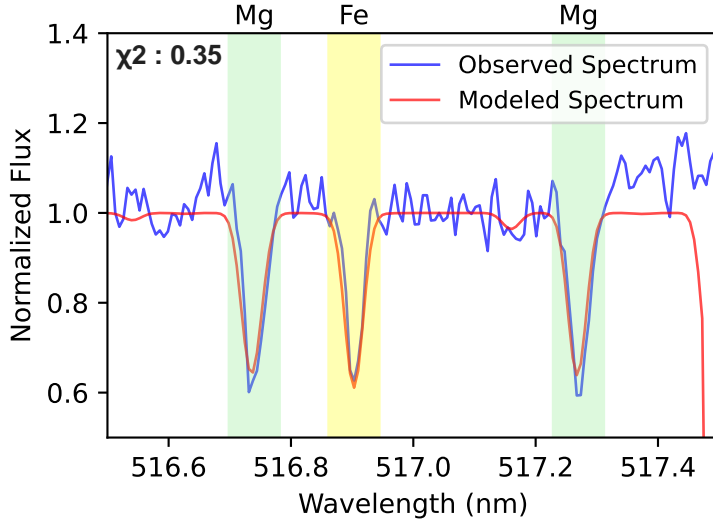


Fig. 3. The observed spectrum, focusing on Mg and Fe lines, is fitted with a model. The observed spectrum is shown in blue, while the fitted model is shown in red. The light green and yellow regions represent the Mg and Fe lines.

astrophysical parameters and individual chemical abundances. In *iSpec*, we used the synthetic spectral fitting method to extract atmospheric parameters and chemical abundances from BSS spectra. This method compares the observed spectrum with synthetic spectra generated on-the-fly (Valenti & Piskunov 1996), focusing on specific spectral features. Utilizing a least-squares algorithm, the differences between the synthetic and observed spectra are minimized to obtain optimal parameters.

The continuum points within a spectrum are identified by applying a median and maximum filter with varying window sizes. The median filter smooths out noise, while the maximum filter disregards deeper fluxes associated with absorption lines (Blanco-Cuaresma et al. 2014). Subsequently, a polynomial fit is employed to model the continuum. Finally, the spectrum is normalized by dividing all flux values by the modelled continuum.

Initially, We determined the radial velocity using two lines of the Mg triplet at 5167.3 Å and 5172.6 Å. After calculating the radial velocities, the spectra were shifted to their rest wavelengths to ensure accurate alignment for further analysis.

The synthetic spectrum was fitted to the observed spectra to determine atmospheric parameters and chemical abundances using *iSpec* (Sarmento et al. 2020; Casamiquela et al. 2022). The synthetic spectra were generated using the ATLAS9.KuruczODFNEW (Castelli & Kurucz 2003) model atmosphere with the SYNTHE (Kurucz 1993; Sbordone et al. 2004) radiative transfer code in *iSpec*, and the Gaia-ESO Survey line list (Heiter et al. 2015; Blanco-Cuaresma 2019). Solar abundances were adopted from (Grevesse & Sauval 1998). Figure 3 illustrates an example of model fitting where an observed spectrum of a BSS (B17) is compared against synthetic spectra, focussing on Mg and

TABLE 2

Mg AND Fe SPECTRAL LINES USED IN THIS STUDY; $\log gf$ DENOTES THE LOGARITHM OF THE PRODUCT OF STATISTICAL WEIGHT AND OSCILLATOR STRENGTH

Element	Peak Wavelength (nm)	$\log gf$
Mg	516.732	-0.931
	517.268	-0.450
Fe	516.903	-1.000

Fe lines. The observed spectrum (blue) is well-matched by the synthetic spectrum (red), achieving a chi-squared value of $\chi^2 = 0.35$. In general, the χ^2 values for the spectral fitting of other BSSs were found to be in the range of 0-1.

To determine the atmospheric parameters, we performed synthetic spectral fitting in two steps, focusing on Mg lines in the first step and Fe lines in the second (see Table 2). The initial parameters for effective temperature (T_{eff}) and surface gravity ($\log g$) were set to 7700 K and 4 dex, respectively, based on the ranges quoted in previous work (6700–8700 K for T_{eff} and 3.6–4.3 dex for $\log g$; (Billi et al. 2023)). The metallicity ([M/H]) was fixed at -1.59 , consistent with the cluster’s [Fe/H] value (Harris 1996). The $v \sin i$ values were sourced from Cosmic-Lab. Initial values for microturbulence (v_{mic}) and macroturbulence (v_{mac}) were estimated using the built-in functions `estimate_vmic` and `estimate_vmac` in `iSpec`, which use empirical relations based on T_{eff} , $\log g$, and [M/H]. These initial values were 2.27 km s^{-1} for v_{mic} and 26.73 km s^{-1} for v_{mac} .

Atmospheric parameters (T_{eff} and $\log g$) were derived independently from Mg and Fe lines. The final T_{eff} and $\log g$ values listed in Table 3 for each BSS were computed as the means of the values derived from Mg and Fe lines, with the standard deviations representing the errors.

Using the final atmospheric parameters, we re-ran the spectral fitting to derive the values of [Mg/Fe] and [Fe/H]. The uncertainties in [Mg/Fe] and [Fe/H] were calculated by propagating the errors in T_{eff} and $\log g$. For this, the abundances were re-computed by varying each atmospheric parameter (T_{eff} , $\log g$) within its upper and lower uncertainty limits while keeping the others fixed. The resulting variations in the abundances were combined in quadrature to estimate the final uncertainties. Given the limited number of spectral lines available, these results should be approximate estimates.

4. RESULTS AND DISCUSSION

Using the methodology provided in § 3, we performed spectral analysis of the BSSs in NGC 3201. The radial velocities, atmospheric parameters (T_{eff} and $\log g$) and chemical abundances derived from the spectra for all 39 BSSs are provided in Table 3.

Figure 4 shows a histogram of radial velocities obtained for the BSSs. We performed a Gaussian fit to determine the average radial velocity for the BSSs as $498.0 \pm 5.3 \text{ km s}^{-1}$. Comparing this with the cluster’s radial velocity of $494.0 \pm 0.2 \text{ km s}^{-1}$ (Harris 1996), the BSSs’ average radial velocity is similar within error.

TABLE 3

ATMOSPHERIC PARAMETERS AND CHEMICAL ABUNDANCES OF THE BSSs. THE VALUES OF $v \sin(i)$ IS TAKEN FROM COSMIC-LAB.

BSS ID	RV (km s ⁻¹)	$v \sin(i)$ (km s ⁻¹)	T _{eff} (K)	log <i>g</i>	[Fe/H]	[Mg/Fe]
B1	503.52	5 ± 2	7112 ± 529	4.5 ± 0.7	-1.47 ± 0.22	-0.14 ± 0.62
B2	502.21	12 ± 2	7830 ± 487	4.9 ± 0.1	-1.22 ± 0.11	1.39 ± 0.57
B3	482.51	13 ± 2	6951 ± 726	4.9 ± 0.1	-1.43 ± 0.33	0.49 ± 0.83
B4	492.60	9 ± 1	6910 ± 517	3.9 ± 0.9	-1.32 ± 0.61	0.32 ± 0.72
B5	493.97	5 ± 1	6260 ± 629	2.6 ± 0.9	-1.28 ± 0.34	-0.07 ± 0.56
B6	498.02	5 ± 1	6962 ± 118	3.6 ± 0.9	-1.04 ± 0.56	1.21 ± 0.46
B7	499.53	25 ± 2	6780 ± 617	3.2 ± 0.9	-1.21 ± 0.42	0.05 ± 0.44
B8	507.22	5 ± 1	7772 ± 771	4.5 ± 0.7	-1.13 ± 0.28	1.36 ± 0.81
B9	493.97	16 ± 3	7724 ± 146	4.5 ± 0.7	-1.40 ± 0.23	1.06 ± 0.23
B10	496.45	5 ± 1	6545 ± 634	3.4 ± 0.9	-1.63 ± 0.46	-0.43 ± 0.65
B11	497.79	16 ± 3	8283 ± 371	4.8 ± 0.3	-1.76 ± 0.11	0.52 ± 0.39
B12	493.97	5 ± 2	6659 ± 697	3.9 ± 0.9	-1.35 ± 0.53	0.46 ± 1.02
B13	509.48	9 ± 3	7040 ± 146	4.9 ± 0.1	-1.15 ± 0.08	0.36 ± 0.16
B14	497.79	5 ± 1	6555 ± 277	3.4 ± 0.6	-1.65 ± 0.31	0.40 ± 0.24
B15	498.02	14 ± 2	6714 ± 723	2.9 ± 0.9	-1.50 ± 0.51	-1.32 ± 0.75
B16	488.24	20 ± 2	7388 ± 772	4.9 ± 0.1	-1.38 ± 0.16	0.05 ± 1.12
B17	490.68	5 ± 2	6717 ± 856	3.3 ± 0.9	-1.96 ± 0.52	-0.80 ± 0.72
B18	498.02	15 ± 2	6899 ± 741	3.4 ± 0.8	-1.77 ± 0.59	-0.04 ± 0.52
B19	499.70	36 ± 4	7735 ± 825	5.0 ± 0.0	-1.40 ± 0.12	-0.03 ± 0.98
B20	501.61	10 ± 3	7202 ± 701	3.7 ± 0.9	-1.22 ± 0.66	-0.20 ± 0.77
B21	495.69	5 ± 2	6490 ± 409	4.0 ± 0.8	-1.67 ± 0.39	0.65 ± 0.66
B22	495.88	5 ± 2	6953 ± 712	4.0 ± 0.9	-1.47 ± 0.50	-0.08 ± 0.97
B23	503.38	9 ± 1	7010 ± 591	3.9 ± 0.9	-1.24 ± 0.52	-0.69 ± 0.59
B24	490.15	6 ± 2	6864 ± 307	4.3 ± 0.9	-1.60 ± 0.43	0.37 ± 0.58
B25	498.02	17 ± 3	8690 ± 673	4.9 ± 0.2	-1.23 ± 0.12	1.89 ± 1.06
B26	493.97	25 ± 3	8373 ± 551	3.0 ± 0.7	-2.36 ± 0.49	0.48 ± 0.52
B27	495.69	35 ± 4	7420 ± 825	4.4 ± 0.5	-1.27 ± 0.25	0.39 ± 0.91
B28	504.13	5 ± 2	7000 ± 343	3.9 ± 0.9	-1.27 ± 0.58	0.35 ± 0.50
B29	492.60	5 ± 2	6823 ± 788	3.9 ± 0.9	-1.14 ± 0.57	-0.02 ± 1.08
B30	503.52	5 ± 2	6898 ± 890	3.6 ± 0.9	-1.13 ± 0.51	-0.03 ± 1.42
B31	498.02	10 ± 1	6564 ± 900	3.0 ± 0.8	-1.38 ± 0.51	-0.70 ± 0.92
B32	498.36	26 ± 2	8419 ± 442	4.0 ± 0.7	-1.60 ± 0.60	0.69 ± 0.63
B33	501.61	5 ± 2	7365 ± 382	4.9 ± 0.2	-1.07 ± 0.09	0.80 ± 0.38
B34	501.84	5 ± 1	7660 ± 666	4.3 ± 0.8	-1.28 ± 0.28	1.37 ± 0.71
B35	499.53	27 ± 3	7877 ± 186	4.2 ± 0.8	-1.69 ± 0.56	1.03 ± 0.52
B36	495.69	13 ± 2	7964 ± 622	4.4 ± 0.9	-1.43 ± 0.32	1.61 ± 0.78
B37	507.22	5 ± 2	7217 ± 400	3.8 ± 0.9	-1.69 ± 0.67	-0.79 ± 0.46
B38	507.22	17 ± 3	8415 ± 367	4.6 ± 0.6	-1.59 ± 0.26	1.61 ± 0.53
B39	501.61	5 ± 2	7059 ± 457	4.2 ± 0.9	-0.97 ± 0.79	0.49 ± 0.71

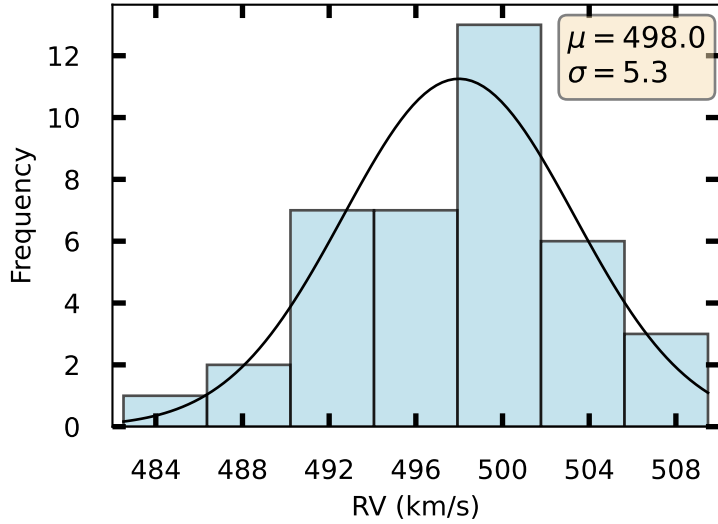
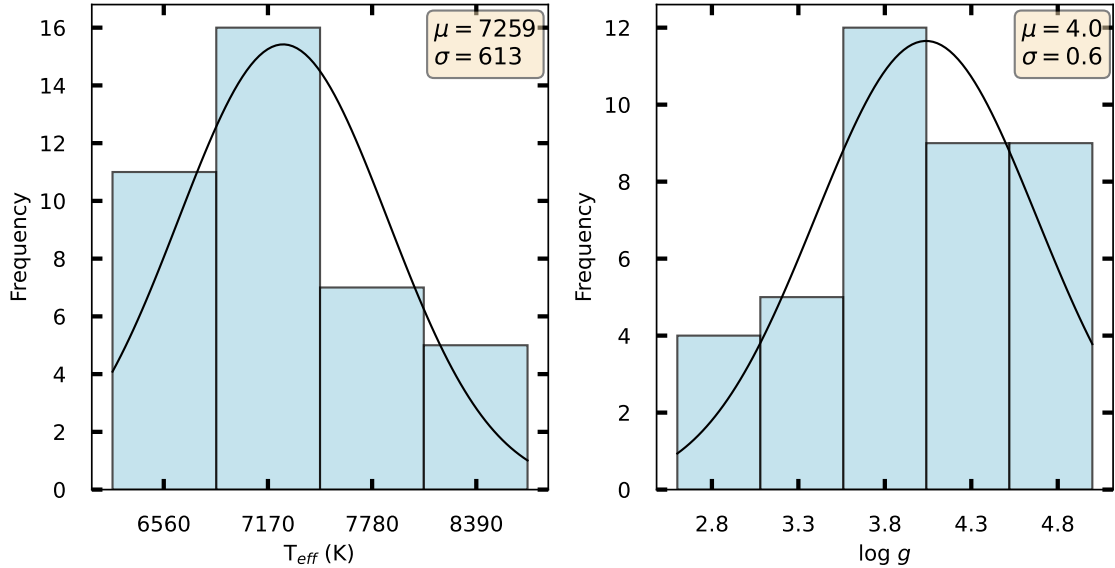


Fig. 4. Histograms of Radial velocity estimated for the 39 BSSs.

Fig. 5. Histograms of T_{eff} and $\log g$ estimated for the BSSs.

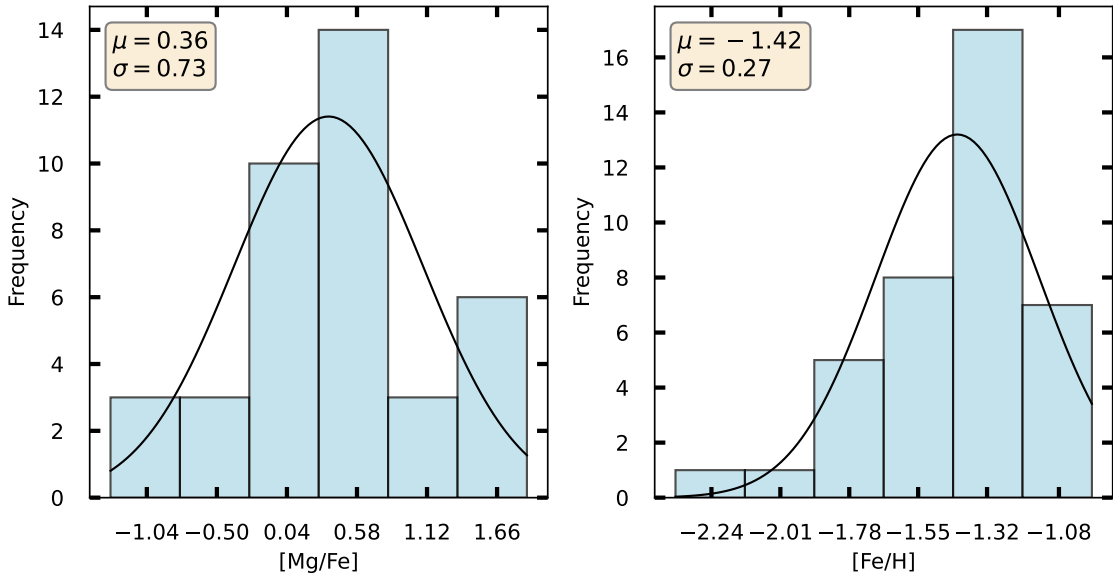


Fig. 6. Histograms of [Mg/Fe] and [Fe/H] values estimated for BSSs.

Figure 5 provides insights into the obtained T_{eff} and $\log g$ values. The range of T_{eff} and $\log g$ for the BSS is 6260 - 8690 K and 2.6 - 5.0, respectively. Billi et al. (2023) quoted the T_{eff} and $\log g$ in the range of 6700-8700 K and 3.6-4.3, respectively, for the BSSs in NGC 3201. Our derived values are also nearly in the same range. The Gaussian fitting to the histogram provides a mean T_{eff} and $\log g$ of the BSSs as 7259 ± 613 K and 4.0 ± 0.6 dex, respectively.

Figure 6 provides histogram plots of the obtained chemical abundances of [Mg/Fe] and [Fe/H]. We performed Gaussian fitting on these distributions to determine the average values of [Mg/Fe] and [Fe/H]. The mean values obtained are $[\text{Mg/Fe}] = 0.36 \pm 0.73$ and $[\text{Fe/H}] = -1.42 \pm 0.27$. Muñoz et al. (2013) performed a detailed chemical abundance analysis of eight red giants in NGC 3201 using high-resolution spectroscopy. They found mean values of $[\text{Fe/H}] = -1.53 \pm 0.01$ and $[\text{Mg/Fe}] = 0.38 \pm 0.03$. These values are comparable with errors in our measurements for the BSSs. However, we observe significant dispersion in our abundance values, likely due to the lower SNR, resolution, and the limited number of available lines. The obtained mean [Fe/H] value of -1.42 ± 0.27 is consistent with the cluster's [Fe/H] value of -1.59 within error.

As mentioned in § 1, two main scenarios have been proposed for forming BSS: mass transfer and stellar collisions leading to mergers. Distinguishing which of these processes gave rise to BSS is challenging. However, chemical abundance analysis of BSS may be the most effective method for differentiating these two formation scenarios. Collisional BSSs are not expected to exhibit abundance anomalies. In contrast, mass transfer BSSs typically show depleted surface abundances of α -elements such as carbon (C), oxygen (O), and magnesium (Mg) (Lovisi et al. 2013). Our derived values for [Mg/Fe] have large uncertainty, which prevents us from making definitive statements

about the formation mechanisms of these BSSs.

While we attempted to identify correlations within the current dataset, no statistically significant relationships could be established. We also looked into the color histogram for the BSSs but no relationship was observed. Nevertheless, the robustness of the present analysis suggests that future studies with broader spectral coverage in NGC 3201 may yield important insights into potential correlations between the chemical abundances and atmospheric parameters of BSSs.

5. CONCLUSIONS

We analyzed the spectra of 39 BSSs in the globular cluster NGC 3201 and derived radial velocity, atmospheric parameters, and chemical abundance of [Mg/Fe] and [Fe/H]. The present study concludes the following.

1. The radial velocity of the 39 BSSs is determined using the Mg and Fe spectral lines, found in the 482.51 - 509.48 km/s range with a mean value of 498.0 ± 5.3 km/s.
2. The T_{eff} and $\log g$ values are found in the range of 6260 - 8690 K and 2.6 - 5.0, respectively, for the BSSs.
3. The abundance values of Mg and Fe are derived using the same lines. The mean value of [Mg/Fe] is estimated as 0.36 ± 0.73 , while the value of [Fe/H] is estimated as -1.42 ± 0.27 .

ACKNOWLEDGEMENTS

We are grateful to Cosmic-Lab, especially Alex Billi and FR. Ferraro, for providing data on BSSs in NGC 3201 and offering insights into spectral corrections.

REFERENCES

Billi, A., Ferraro, F. R., Mucciarelli, A., Lanzoni, B., Cadelano, M., Monaco, L., Mateo, M., Bailey, J. I., Reiter, M., & Olszewski, E. W. 2023, ApJ, 956, 124

Blanco-Cuaresma, S. 2019, MNRAS, 486, 2075

Blanco-Cuaresma, S., Soubiran, C., Heiter, U., & Jofré, P. 2014, A&A, 569, A111

Casamiquela, L., Gebran, M., Agüeros, M. A., Bouy, H., & Soubiran, C. 2022, AJ, 164, 255

Castelli, F. & Kurucz, R. L. Modelling of Stellar Atmospheres, ed. , N. PiskunovW. W. Weiss & D. F. Gray, Vol. 210, A20

Ferraro, F. R., Sabbi, E., Gratton, R., Piotto, G., Lanzoni, B., Carretta, E., Rood, R. T., Sills, A., Fusi Pecci, F., Moehler, S., Beccari, G., Lucatello, S., & Compagni, N. 2006, ApJ, 647, L53

Fiorentino, G., Lanzoni, B., Dalessandro, E., Ferraro, F. R., Bono, G., & Marconi, M. 2014, ApJ, 783, 34

Gilliland, R. L., Bono, G., Edmonds, P. D., Caputo, F., Cassisi, S., Petro, L. D., Saha, A., & Shara, M. M. 1998, ApJ, 507, 818

Grevesse, N. & Sauval, A. J. 1998, Space Sci. Rev., 85, 161

Harris, W. E. 1996, AJ, 112, 1487

Heiter, U., Lind, K., Asplund, M., Barklem, P. S., Bergemann, M., Magrini, L., Masseron, T., Mikolaitis, Š., Pickering, J. C., & Ruffoni, M. P. 2015, Phys. Scr, 90, 054010

Hills, J. G. & Day, C. A. 1976, *Astrophys. Lett.*, 17, 87

Kurucz, R. 1993, Robert Kurucz CD-ROM, 18

Leonard, P. J. T. 1989, *AJ*, 98, 217

Lombardi Jr., J. C., Rasio, F. A., & Shapiro, S. L. 1995, *ApJ*, 445, L117

Lovisi, L., Mucciarelli, A., Ferraro, F. R., Lucatello, S., Lanzoni, B., Dalessandro, E., Beccari, G., Rood, R. T., Sills, A., Fusi Pecci, F., Gratton, R., & Piotto, G. 2010, *ApJ*, 719, L121

Lovisi, L., Mucciarelli, A., Lanzoni, B., Ferraro, F. R., & Dalessandro, E. 2013, *Mem. Soc. Astron. Italiana*, 84, 232

McCrea, W. H. 1964, *MNRAS*, 128, 147

Monty, S., Puzia, T. H., Miller, B. W., Carrasco, E. R., Simunovic, M., Schirmer, M., Stetson, P. B., Cassisi, S., Venn, K. A., Dotter, A., Goudfrooij, P., Perina, S., Peshev, P., Sarajedini, A., & Taylor, M. A. 2018, *ApJ*, 865, 160

Muñoz, C., Geisler, D., & Villanova, S. 2013, *MNRAS*, 433, 2006

Mucciarelli, A., Lovisi, L., Ferraro, F. R., Dalessandro, E., Lanzoni, B., & Monaco, L. 2014, *ApJ*, 797, 43

Nardiello, D., Libralato, M., Piotto, G., Anderson, J., Bellini, A., Aparicio, A., Bedin, L. R., Cassisi, S., Granata, V., King, I. R., Lucertini, F., Marino, A. F., Milone, A. P., Ortolani, S., Platais, I., & van der Marel, R. P. 2018, *MNRAS*, 481, 3382

Sandage, A. R. 1953, *AJ*, 58, 61

Sarmento, P., Delgado Mena, E., Rojas-Ayala, B., & Blanco-Cuaresma, S. 2020, *A&A*, 636, A85

Sbordone, L., Bonifacio, P., Castelli, F., & Kurucz, R. L. 2004, *Memorie della Societa Astronomica Italiana Supplementi*, 5, 93

Shara, M. M., Saffer, R. A., & Livio, M. 1997, *ApJ*, 489, L59

Stetson, P. B., Pancino, E., Zocchi, A., Sanna, N., & Monelli, M. 2019, *MNRAS*, 485, 3042

Valenti, J. A. & Piskunov, N. 1996, *A&AS*, 118, 595

Vasiliev, E. & Baumgardt, H. 2021, *MNRAS*, 505, 5978